A Convex Allocation Framework for Singularity Avoidance in Control Moment Gyro Clusters

Hugo André Chamusca Pereira
hugo.c.pereira@tecnico.ulisboa.pt

Instituto Superior Técnico, Universidade de Lisboa, Portugal

November 2022

Abstract: In robotics, the occurrence of singularities typically results in a loss of a degree of freedom. For spacecrafts employing control moment gyro clusters, singularities may occur due to the alignment of the gimbals, which inhibits the creation of torque in at least one direction. This translates into a loss of control authority that has a direct impact on the spacecraft's attitude control system. In this work, an optimal allocation framework for singularity avoidance is proposed. The presented solution aims to provide a singularity-robust allocation scheme that can be used as an add-on to a conventional attitude controller. This algorithm resorts to the model predictive control framework to predict the future states of the gimbals and, subsequently, take control actions that lead to singularity-free configurations while minimizing the control energy spent. The use of a redundant actuator makes it possible to avoid singularities while the system meets the torque references defined by the controller. Moreover, a novel, computationally efficient and numerically robust, singularity metric is derived to assess the proximity of a singularity. This function overcomes the complexity of the standard literature solutions, such as the condition number, and can be integrated as a linear constraint in a convex optimization problem. Finally, the proposed approach is applied to a two-dimensional control moment gyro cluster in a simulation environment. It is verified that the system is capable of avoiding all of the internal singularities of the cluster at a relatively low computational expense.

Keywords: control moment gyros; singularities; action governor; model predictive control; convexity.

1. Introduction

1.1. *Motivation*

Control momentum gyros (CMGs) are angular momentum storage devices that can be used as steering actuators for spacecraft attitude control. A control moment gyro consists of a spinning rotor, or flywheel, and one or more motorized gimbals that tilt the rotor's angular momentum to create torque on the spacecraft. Most CMGs contain a single gimbal, which allows the creation of torque in a plane normal to the gimbal spinning axis. A spacecraft employing a cluster of single gimbal CMGs (SGCMGs) requires at least three of these devices for attitude control. Indeed, there are as many degrees of freedom as gimbals. Yet, spacecrafts typically employ at least one extra CMG for redundancy.

While gimbaling a flywheel, there is the chance of witnessing alignments in the system. When these situations happen, the spacecraft is not able to produce torque in certain directions. These configurations are known as singularities and are related to the kinematics of a robotic arm that encounters motion limits on the end-effector due to joint alignments [1]. Also denoted by gimbal-lock, these special configurations happen when the spacecraft is holding the maximum amount of angular momentum in one direction - in this case, referred to as saturation singularities, or when the spacecraft loses controllability due to an anti-parallel alignment in the system. Singularities constitute an issue of major concern as they have a direct impact on the spacecraft's actuation capability, and therefore can affect the spacecraft's orientation during a manoeuvre. Depending on their magnitude, singularities can be considered critical for missions requiring high-pointing capabilities, and therefore, should be avoided.

1.2. *Objectives*

The goal of this letter is to provide an attitude control framework for singularity avoidance. This can be accomplished by first understanding the different types of singularities of a specific CMG cluster, concluding about their influence on the spacecraft's motion, and finding a way of minimizing their effect.

1.3. *Literature review*

Several allocation algorithms have been studied to determine the inputs to the gimbals, i.e., the gimbal rates. The pseudoinverse steering law, known as the Moore-Penrose pseudoinverse, is one of the simplest and most frequent steering laws. This minimal two-norm approach receives the torques from the controller and computes the gimbal rates using the right pseudoinverse method. Obviously, this method does not contemplate the proximity of a singularity. Among the existing solutions that acknowledge the existence of singularities, one can distinguish singularity escape algorithms from singularity

avoidance algorithms. Some approaches have both capabilities, as depicted in Fig. 1 [1].

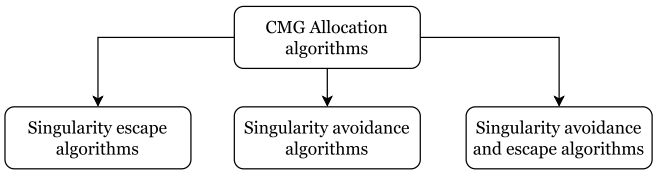

Fig. 1: Types of CMG allocation algorithms.

Singularity escape algorithms aim to overcome singularities through small torque deviations from the command torque. The purpose of these algorithms is to keep the conditioning of the actuator's Jacobian as small as possible. To achieve this, an inexact mapping, from the command torque to the gimbal rates, through a pseudo-inverse method is employed. Although these techniques have been proven effective to escape from singularities, these methods are likely impractical when attitude tracking accuracy is of primary importance. In these cases, where torque matching is strictly necessary, other alternatives that do not explore the use of torque error are often preferred.

Some types of singularities, i.e. internal singularities, offer the possibility of avoidance without the introduction of a torque error. Singularity avoidance algorithms make use of null motion to avoid such singularities. This is possible due to the use of a redundant CMG, that allows for infinite different CMG configurations for every command torque. Nevertheless, some singularities, namely external singularities, cannot be avoided through the use of null motion. In these cases a torque error is acceptable to escape the singularity effect. Many algorithms that comprise both singularity avoidance and escape capabilities have been recently studied.

Optimal control approaches are commonly employed for singularity avoidance and escape. A research done by H. Leeghim et al. [2] computes the optimal gimbal rates via a one-step-ahead strategy. This method uses a mathematical model of the system to predict the state of the gimbals one-step further in time. Receding horizon (RH) control was extensively studied by K. Takada and H. Kojima in [3]. This work tackles the low manoeuvring time associated with trajectories that pass through or near singularities, and are therefore critical for agile missions. A model predictive controller is described in [4] to compute the gimbal rates that minimize the torque error over the prediction horizon. This strategy computes the gimbal rates in an integrated fashion, merging both the controller and control allocation steps into a single optimization problem. A nonlinear model predictive controller for attitude tracking of constant references with consideration of singularities was proposed in [5]. This approach, however, exhibits a very complex formulation, leading to very high computational times. In [6] and [7] heurisitic search algorithms have been derived for gimbal path planning. In the first, rapidly-exploring random trees are considered in tandem with a classical steering law to manoeuvre the spacecraft along a path that minimizes the occurrence of singularities. In the second, a global search algorithm, that determines the null motion added upon the singularity robust inverse steering law, was derived. Machine learning (ML) approaches are also becoming popular in spacecraft attitude control. A work published by C. Papakonstantinous et al. [8] employed ML techniques for singularity avoidance with some promising results.

Leading-edge research has mostly focused on the development of steering laws for both singularity avoidance and escape. Optimal control strategies are capable of both and allow for constraint handling, which is paramount for achieving optimal performance while accounting for the physical limitations of the actuators. Nonetheless, optimal control algorithms are usually computationally heavy and inefficient. The formulations can sometimes be complex and highly nonlinear, leading to non-convex optimization problems. Given this, the solution proposed in this letter aims to fill the gap that separates high performance and low computational effort. An end-to-end controller that directly computes gimbal rate commands given the attitude error does not generally cope with these requirements. Therefore, there is a strong commitment throughout this work to find a decoupled and complementary strategy to a known standard controller.

1.4. *Contributions*

The main contributions of this letter are as follows:

- A closed-form description of the singularity envelope is accomplished. For some CMG clusters, the singularities are organized in lines in the gimbal space. This information is leveraged for singularity avoidance by assessing the Euclidean distance between the gimbals and the closest singularity in the envelope. According to the best of the author's knowledge, this is the first time that the distance to the singularities is exploited for singularity avoidance.

- A novel algorithm for CMG allocation is derived. It consists of an add-on allocation technique to a literature controller, that receives the torques computed by the controller, and outputs a sequence of gimbal rates that lead to singularity-free gimbal configurations. This solution resorts to the model predictive control framework and employs a singularity term that considers the Euclidean distance to the closest singularity, resulting in a convex optimization problem.

1.5. *Notation*

Throughout this letter, math symbols and letters are represented in italic. Scalar variables and constants are represented in either small or capital letters, vectors are represented in small boldface letters, and matrices are represented in capital boldface letters. In particular, $\boldsymbol{I}_n$ denotes the $n \times n$ identity matrix, and $diag(a_1, ..., a_N)$ denotes the diagonal matrix whose diagonal entries are given by $a_1, ..., a_N$. The i-th element of the vector $\boldsymbol{v}$ is denoted by v_i, and the entry (i, j) of a matrix $\boldsymbol{M}$ is denoted by M_{ij}.

For a square symmetric matrix $\boldsymbol{P}$, $\boldsymbol{P} \succ 0$ and $\boldsymbol{P} \succeq 0$ are used to indicate that $\boldsymbol{P}$ is positive-definite

and positive-semidefinite, respectively. The operators $\|\cdot\|_2$ and $\|\cdot\|_\infty$ are used to indicate the 2-norm and the ∞-norm of a vector, respectively, and the operator $\|\cdot\|_S$ is equivalent to $\|\cdot\|_S = \sqrt{(\cdot)^T \boldsymbol{S}(\cdot)}$.

2. Background

2.1. *Control moment gyro*

A CMG creates gyroscopic torque by gimbaling a flywheel that is generally spinning at a constant speed. Accordingly, the output torque of a CMG, $\boldsymbol{t}$, is given by

$$\boldsymbol{t} = \frac{d\boldsymbol{h}}{dt} = \boldsymbol{h} \times \dot{\boldsymbol{\gamma}}, \tag{1}$$

where $\boldsymbol{h}$ denotes the CMG angular mometum and $\dot{\boldsymbol{\gamma}}$ represents the gimbal spinning rate [9]. Fig. 2 illustrates the schematics of a CMG.

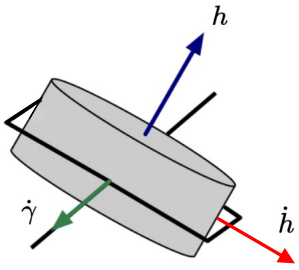

Fig. 2: Control moment gyro (Adapted from [10]).

2.2. *Action Governor*

Consider a system represented by the discrete-time model

$$\boldsymbol{x}(k+1) = f_d(\boldsymbol{x}(k), \boldsymbol{u}(k)), \tag{2}$$

where $\boldsymbol{x}(k) \in \mathbb{R}^m$ represents the system state at the discrete-time instant k, with $k \in \mathbb{R}_0^+$, and $\boldsymbol{u}(k) \in \mathbb{R}^n$ represents the control input. It is assumed that the nominal control policy

$$\boldsymbol{u}_\phi(k) = \phi(\boldsymbol{x}(k), \boldsymbol{r}(k), k) \tag{3}$$

has been defined for the system (2), where $\boldsymbol{r} \in \mathbb{R}^p$ represents the reference signal. The control policy ϕ may be linear, nonlinear, time-invariant, or time-variant. Furthermore, consider that the system state $\boldsymbol{x}(k)$ is subject to an exclusion zone requirement of the form

$$\boldsymbol{x}(k) \notin \mathcal{X}_0, \ , \forall k \in \mathbb{Z}_0^+, \tag{4}$$

where the set of all feasible $\boldsymbol{x}$ is denoted by $\mathcal{X}$. The nominal control policy does not necessarily contemplate the exclusion zone requirement (4). Therefore, there may be situations where the system state lies in $\mathcal{X}_0$, which may lead to undesired consequences. The goal of the algorithm proposed in [11] aims to enforce (4) by monitoring and minimally modifying the nominal input $\boldsymbol{u}_\phi$ when necessary. This is realized through an add-on supervisory scheme, referred to as Action Governor, as depicted in Fig. 3.

The AG consists of an online constrained optimization problem of the form

$$\begin{aligned} &\underset{\boldsymbol{u}(k) \in \mathcal{U}}{\text{minimize}} && \|u(k) - u_\phi(k)\|_S^2 && \text{(5a)} \\ &\text{subject to} && f_d(\boldsymbol{x}(k), \boldsymbol{u}(k)) \in \mathcal{X} \backslash \mathcal{X}_0, && \text{(5b)} \end{aligned}$$

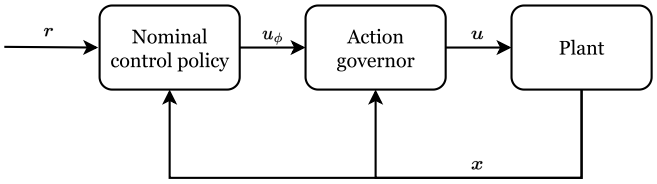

Fig. 3: Action governor scheme.

where $\mathcal{U}$ represents the range of control inputs, $\boldsymbol{S}$ is a positive-definite matrix, and (5a) is used to penalize the difference between the nominal control command $\boldsymbol{u}_\phi$ and the modified control command $\boldsymbol{u}$ that satisfies (5b) [11].

2.3. *Model Predictive Control*

Model predictive control (MPC) is an advanced control method typically used to control a system while satisfying a set of constraints. MPC uses a mathematical model to predict the future behaviour of the system and take control actions accordingly. These control actions, that drive the system to the setpoints, result from solving a constrained optimization problem (see Fig. 4). The inputs to the MPC are a sequence of setpoints over a finite duration time-window.

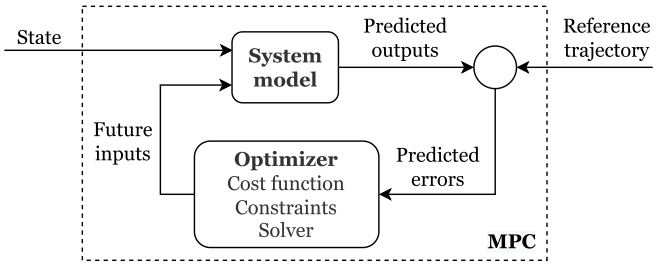

Fig. 4: MPC block.

The operating principle of a MPC is described as follows:

- The outputs for a given prediction horizon N_p, at the time instant k, are predicted sequentially using a dynamic model of the system. The predicted outputs depend on the state of the system and the computed control signals up to the time instant $k-1$.
- The sequence of future control actions is determined by optimizing a cost function under specific constraints. The cost function usually comprises a term that penalizes deviations from the setpoint over the prediction horizon and a term to regularize the control effort. The constraints of the optimization problem include the model equations that dictate the next state of the system given its current state and the input. These may also include saturation functions, input rate limiters, or even state restrictions. Usually, state constraints can be relaxed by being penalized in the cost function instead.
- The first control action in the control sequence $\boldsymbol{u}$ is applied to the system while the remaining control signals are discarded. On the next sampling instant, the control sequence is re-computed for a different

state $\boldsymbol{x}$. The control horizon, N_c, dictates the number of optimized control actions. If the control horizon is smaller than the prediction horizon, the last computed input is kept constant for the remaining length of the horizon [12].

3. Model definition

3.1. *Actuator dynamics*

A CMG cluster consisting of three control moment gyros is considered throughout this document. As shown in Fig. 5, the cluster is arranged in a way such that every CMG sits on a vertex of an equilateral triangle. This is a simple model, not commonly used in real spacecrafts as it only provides roll and pitch control. However, it contains a convenient singularity envelope that will be further explored to demonstrate the potential of the proposed approach. To compensate for yaw control and achieve full 3-dimensional controllability, a reaction wheel is later added to the z-direction.

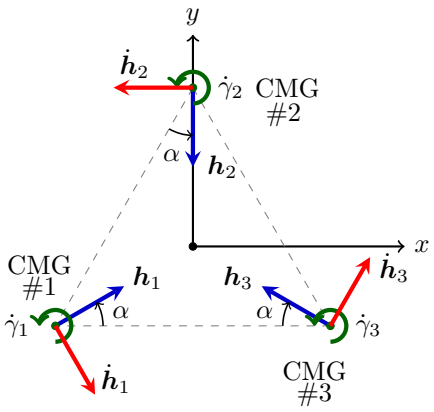

Fig. 5: Triangular cluster of CMGs.

Designating the momentum of the i-th CMG by $\boldsymbol{h}_i$, the angular momentum of the entire system is given by the sum of the angular momentum produced by each CMG, i.e.

$$\boldsymbol{h} = \boldsymbol{h}_1 + \boldsymbol{h}_2 + \boldsymbol{h}_3, \tag{6}$$

which results in

$$\begin{aligned}\boldsymbol{h} = h_0 \begin{pmatrix} \cos(\alpha+\gamma_1) \\ \sin(\alpha+\gamma_1) \end{pmatrix} + h_0 \begin{pmatrix} \sin\gamma_2 \\ -\cos\gamma_2 \end{pmatrix} \\ + h_0 \begin{pmatrix} -\cos(\alpha-\gamma_3) \\ \sin(\alpha-\gamma_3) \end{pmatrix} \in \mathbb{R}^2,\end{aligned} \tag{7}$$

where $h_0 \in \mathbb{R}$ is momentum magnitude of each CMG, $\alpha = 30°$, and $\boldsymbol{\gamma} \in \mathbb{R}^3$ is the gimbal angle vector. The time derivative of the angular momentum can be determined by applying the chain rule to (7), yielding

$$\dot{\boldsymbol{h}}(\boldsymbol{\gamma}) = \frac{\partial \boldsymbol{h}}{\partial \boldsymbol{\gamma}} \frac{\partial \boldsymbol{\gamma}}{\partial t} = \boldsymbol{J}(\boldsymbol{\gamma})\dot{\boldsymbol{\gamma}}, \tag{8}$$

where $\boldsymbol{J} \in \mathbb{R}^{2\times 3}$ represents the Jacobian given by

$$\boldsymbol{J}(\boldsymbol{\gamma}) = h_0 \begin{pmatrix} -\sin(\alpha+\gamma_1) & \cos\gamma_2 & -\sin(\alpha-\gamma_3) \\ \cos(\alpha+\gamma_1) & \sin\gamma_2 & -\cos(\alpha-\gamma_3) \end{pmatrix}. \tag{9}$$

3.2. *Satellite dynamics*

Control moment gyros exploit the principle of conservation of angular momentum to steer the spacecraft. The motion of a satellite equipped with an arbitrary system of CMGs can be expressed by

$$\dot{\boldsymbol{h}}_s + \boldsymbol{\omega} \times \boldsymbol{h}_s = \boldsymbol{\tau}, \tag{10}$$

where $\boldsymbol{h}_s \in \mathbb{R}^3$ denotes the angular momentum respective to the satellite motion, $\boldsymbol{\omega}$ is the satellite angular velocity, and $\boldsymbol{\tau} \in \mathbb{R}^3$ denotes the external torques applied on the spacecraft. The satellite's angular momentum is defined as

$$\boldsymbol{h}_s = \boldsymbol{I}_s\boldsymbol{\omega} + \boldsymbol{h}, \tag{11}$$

where $\boldsymbol{I}_s \in \mathbb{R}^{3\times 3}$ designates the matrix of inertia of the spacecraft, and $\boldsymbol{h} \in \mathbb{R}^3$ represents the angular momentum produced by the CMG system. Since spacecrafts can be regarded as rigid bodies, the time derivative of $\boldsymbol{h}_s$ with respect to the body axis simplifies to

$$\frac{d\boldsymbol{h}_s}{dt} = \underbrace{\dot{\boldsymbol{I}}_s\boldsymbol{\omega}}_{=0} + \boldsymbol{I}_s\dot{\boldsymbol{\omega}} + \dot{\boldsymbol{h}} = \boldsymbol{I}_s\dot{\boldsymbol{\omega}} + \dot{\boldsymbol{h}}. \tag{12}$$

Substituting (12) and (11) in (10), yields

$$\boldsymbol{I}_s\dot{\boldsymbol{\omega}} + \dot{\boldsymbol{h}} + \boldsymbol{\omega} \times (\boldsymbol{I}_s\boldsymbol{\omega} + \boldsymbol{h}) = \boldsymbol{\tau}. \tag{13}$$

Finally, solving (13) with respect to the satellite's angular acceleration, one obtains

$$\dot{\boldsymbol{\omega}} = \boldsymbol{I}_s^{-1}(-\dot{\boldsymbol{\omega}} \times \boldsymbol{I}_s\dot{\boldsymbol{\omega}} - \dot{\boldsymbol{h}} - \boldsymbol{\omega} \times \boldsymbol{h} + \boldsymbol{\tau}). \tag{14}$$

3.3. *Satellite kinematics*

The kinematics of the satellite can be described using unit quaternions. In aerospace applications, it is common to use a special quaternion for attitude representation, denoted by $\bar{\boldsymbol{q}}$, whose derivative is given by

$$\dot{\bar{\boldsymbol{q}}} = \frac{1}{2}\boldsymbol{\Omega}(\boldsymbol{\omega})\bar{\boldsymbol{q}}, \tag{15}$$

where

$$\boldsymbol{\Omega}(\boldsymbol{\omega}) = \begin{pmatrix} 0 & -\omega_1 & -\omega_2 & -\omega_3 \\ \omega_1 & 0 & \omega_3 & -\omega_2 \\ \omega_2 & -\omega_3 & 0 & \omega_1 \\ \omega_3 & \omega_2 & -\omega_1 & 0 \end{pmatrix}. \tag{16}$$

The scalar component of the quaternion is designated by q_0, and its vectorial part is designated by $\boldsymbol{q}$.

4. Singularity analysis

In robotics, a singularity is defined as a configuration where at least one degree of freedom is lost. Since the output of the CMG system represents torques, it becomes impossible to produce torque in a given direction under the presence of a singularity. Mathematically, this is evaluated by the rank of the Jacobian. Therefore, there is a singularity whenever

$$\operatorname{rank}(\boldsymbol{J}(\boldsymbol{\gamma})) < \min(m, n), \tag{17}$$

giving that $\boldsymbol{J}(\boldsymbol{\gamma}) \in \mathbb{R}^{m\times n}$. For non-square matrices where $m < n$, this is equivalent to verifying when the determinant of $\boldsymbol{J}\boldsymbol{J}^T$ equals zero, i.e.,

$$\det(\boldsymbol{J}\boldsymbol{J}^T) = 0. \tag{18}$$

4.1. *Singularities in the triangular cluster of CMGs*

The rank of the Jacobian, for the triangular CMG system, is equal to two in non-singular circumstances. This is the maximum rank it can take, as this matrix has two rows and three columns. When the system meets a singularity, the Jacobian becomes rank deficient. In this scenario, the rank of the Jacobian drops to one, making it impossible to create torque in 2-dimensions. Since CMGs comprise flywheels that are permanently at a constant speed, it is impossible to witness rank-0 singularities in SGCMG systems. The singularities of the triangular CMG system can be classified in 3h or 1h, depending on the orientation of the gimbals. Also known by saturation singularities, 3h singularities occur when the system is exerting the maximum amount of torque in a single direction. On the other hand, 1h singularities happen when the direction of flywheels is the same, just like in the 3h singularities, but one CMG is spinning in the opposite direction of the other two. An example of a 3h singularity is provided in Fig. 6.

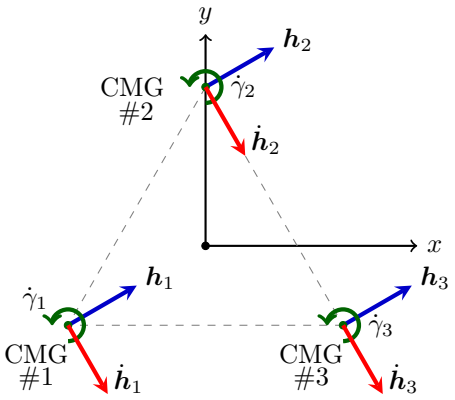

Fig. 6: Example of a 3h singularity.

To determine the whole singularity envelope, one has to solve (18). Since the expression for the determinant is quite complex to solve analytically, it is easier to break down the determinant of $\boldsymbol{J}\boldsymbol{J}^T$ into the sum of the determinants of its submatrices. Indeed, according to the Cauchy-Binet theorem [13], the determinant of $\boldsymbol{J}\boldsymbol{J}^T$ is equivalent to

$$\det(\boldsymbol{J}\boldsymbol{J}^T) = \sum_{i=1}^{n} d_i^2, \tag{19}$$

where $d_i = \det(\boldsymbol{J_i})$ are the Jacobian minors of order m and $\boldsymbol{J_i} = \boldsymbol{J}$ with the i-th column removed. The computation of each determinant, for the triangular CMG system, is straightforward, yielding

$$d_1^2 = \frac{h_0^4}{2}\cos\left(2\gamma_2 - 2\gamma_3 + 2\alpha\right) + \frac{h_0^4}{2}, \tag{20a}$$

$$d_2^2 = \frac{h_0^4}{2}\cos\left(2\gamma_3 - 2\gamma_1 + 2\alpha\right) + \frac{h_0^4}{2}, \tag{20b}$$

$$d_3^2 = \frac{h_0^4}{2}\cos\left(2\gamma_1 - 2\gamma_2 + 2\alpha\right) + \frac{h_0^4}{2}. \tag{20c}$$

To verify (18), every determinant d_i has to be zero. This results in the singularity lines defined by

$$\gamma_1 = \gamma_3 - \frac{\pi}{3} + k_\beta\pi, \quad k_\beta \in \mathbb{Z}, \tag{21a}$$

and

$$\gamma_2 = \gamma_3 + \frac{\pi}{3} + k_\gamma\pi, \quad k_\gamma \in \mathbb{Z}, \tag{21b}$$

where $\gamma_3 \in \mathbb{R}$. Some of these singularity lines represent 1h singularities, while others represent 3h singularities. The plot shown in Fig. 7 depicts the different singularities for the gimbal space where

$$\gamma_i \in [-\pi, \pi] \text{ rad}, \quad \forall i \in \{1, 2, 3\}. \tag{22}$$

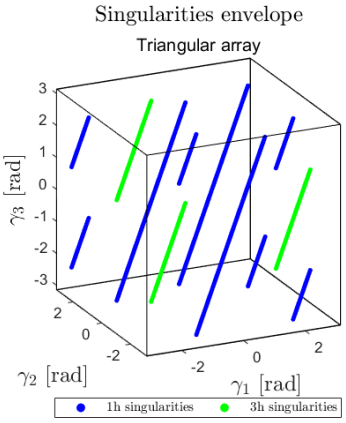

Fig. 7: Singularities envelope.

4.2. *Torque envelopes*

The torque envelopes for both a singular and a non-singular gimbal configurations are analysed next via the singular value decomposition (SVD) of the Jacobian.

For the non-singular gimbal configuration $\boldsymbol{\gamma} = (0, 0, 0)^T$, represented in Fig. 5, the Jacobian takes the form

$$\boldsymbol{J}(\boldsymbol{\gamma}) = h_0 \begin{pmatrix} -0.5000 & 1.000 & -0.5000 \\ 0.8660 & 0 & -0.8660 \end{pmatrix}, \tag{23}$$

being full rank, i.e., $\text{rank}(\boldsymbol{J}(\boldsymbol{\gamma})) = 2$. In fact, the SVD of the Jacobian suggests that both singular values are non-zero and even share the same value, i.e. $\sigma_1 = \sigma_2 = 1.225h_0$. Since both singular values are non-null, there are no singular directions in (23), meaning that for this gimbal configuration, torque is available in any direction.

For the singular gimbal configuration shown in Fig. 6, where $\boldsymbol{\gamma}_s = (0, 2\pi/3, -2\pi/3)^T$, the Jacobian is given by

$$\boldsymbol{J}(\boldsymbol{\gamma}_s) = h_0 \begin{pmatrix} -0.5000 & -0.5000 & -0.5000 \\ 0.8660 & 0.8660 & 0.8660 \end{pmatrix}, \tag{24}$$

having two linearly dependent rows. In this case, the rank of the Jacobian equals one, and its SVD contains a null singular value. The singular direction, that has magnitude zero, is given by $\boldsymbol{u} = (-0.8660, -0.5000)^T$. Regardless of the magnitude of the gimbal inputs, the torque produced by the system will be zero along the singular direction $\boldsymbol{u}$. Indeed, if one defines a gimbal input envelope in $\mathbb{R}^3$, where

$$\dot{\gamma}_i \in [-1.5, 1.5] \text{ rad/s}, \quad \forall i \in \{1, 2, 3\}, \tag{25}$$

and map it to torques via (8), it becomes possible to visualize the torque envelopes for both non-singular and singular gimbal configurations. These plots are presented

in Figs. 8 and 9, respectively, and suggest that torques are possible in every 2D direction for the non-singular gimbal configuration, whereas torques are only feasible along the non-singular direction for the singular gimbal configuration.

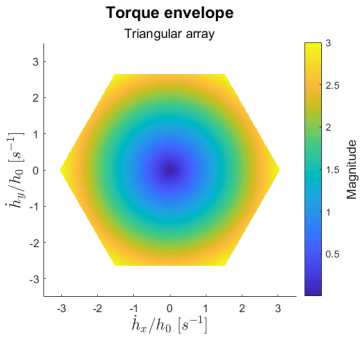

Fig. 8: Torque envelope for the non-singular configuration.

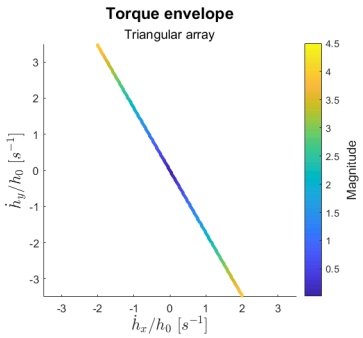

Fig. 9: Torque envelope for the singular configuration.

4.3. *Vicinity of a singularity*

In the previous section, it became clear that when the system crosses a singularity, torque is lost in at least one direction regardless the input given to the gimbals. For real actuators, this is even more problematic as the gimbal rates are physically limited. In fact, as the system approaches a singularity, the inputs to the gimbals become larger in order to cope with the torque required by the controller. The system can only match the commanded torque until the point where it is not further possible to create torque by increasing the speed of the gimbals. This situation typically happens in the vicinity of a singularity and should be avoided as torque matching can no longer be verified. Therefore, the problem of avoiding singularities becomes more complex, since now there is the need to avoid not only the singularity, but also to prevent the system from entering its neighborhood.

5. Controller design and control allocation

5.1. *Singularity metrics*

To design a controller for singularity avoidance, the system has to be able to sense the proximity of a singularity. This information is paramount as it allows the system to take control actions that lead to singularity-free gimbal states. As mentioned in Section 4.3, when the system enters the vicinity of a singularity, the gimbal inputs become larger in an effort to meet the desired torque. Indeed, the 2-norm and the ∞-norm of the gimbal rate vector can be useful metrics to analyse the closeness of a singular state, as their value increases whenever the system approaches a singularity. However, singularities can be hard to discern in situations where the gimbal inputs are large due to the nature of the control torques. Indeed, if the torques are not properly regulated, they might convert into large gimbal rates that can be mistaken for singularities. Yet, limiting the control torques beyond the physical limitations of the actuators is not usually desired, as by doing so, the actuation capability of the satellite decreases. For these reasons, different metrics to evaluate the proximity of a singularity, in an explicit form, have been studied. The manipulability index, defined as

$$m = \sqrt{det(\boldsymbol{J}\boldsymbol{J}^T)}, \tag{26}$$

and the condition number, defined as

$$c = \frac{\sigma_{\max}}{\sigma_{\min}}, \tag{27}$$

where $\sigma_{\max}$ and $\sigma_{\min}$ represent the largest and smallest singular values of the Jacobian, respectively, are the most standard metrics to evaluate the proximity of a singularity. When the system approaches a singularity, m tends to zero, and c tends to infinity as $\sigma_{\min}$ tends to zero. Even though intuitive, these approaches are computationally expensive as they require an online computation of the determinant or the singular values of $\boldsymbol{J}\boldsymbol{J}^T$.

In this letter, a novel, numerically robust and efficient, singularity metric is derived. Start by examining the singularities in a 2-dimensional space. Designating the minimum required distance to a given singularity by κ, one can define a circular exclusion zone centered at the singularity γ_s with radius κ, as depicted in Fig. 10. The

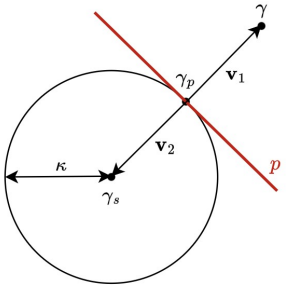

Fig. 10: Exclusion requirement for the 2D case.

exclusion requirement is verified whenever the gimbals, $\boldsymbol{\gamma}$, satisfy

$$\underbrace{(\boldsymbol{\gamma}-\boldsymbol{\gamma}_p)^T}_{\boldsymbol{v}_1^T}\underbrace{(\boldsymbol{\gamma}_s-\boldsymbol{\gamma}_p)}_{\boldsymbol{v}_2} \leq 0, \tag{28}$$

where $\boldsymbol{\gamma}_p$ denotes the projection of the gimbal vector on the exclusion zone boundary, and is calculated by

$$\boldsymbol{\gamma}_p = \boldsymbol{\gamma}_s + \kappa\frac{\boldsymbol{\gamma}-\boldsymbol{\gamma}_s}{\|\boldsymbol{\gamma}-\boldsymbol{\gamma}_s\|_2}. \tag{29}$$

These results are applicable to n-dimensions and can be leveraged for singularity avoidance in many different systems. Before applying (28) and (29), one has to know, at

any given time, the closest singularity in the system. As the singularities are arranged in 3D lines for the triangular CMG cluster (see Fig. 7), the closest point in a singularity line consists of the orthogonal projection of $\boldsymbol{\gamma}$ on the line. Therefore, the closest singularity in the system is achieved by finding the minimum distance between the gimbals and all of the lines contained in the singularity envelope. This can be leveraged to reduce the memory space used to store the location of the singularities, by storing only the information about the equations that describe the singularity lines. Besides this, the number of equations can be minimized by wrapping the gimbal angles to the interval $[-\pi, \pi]$. In this way, only the information regarding the singularity lines contained in the interval $[-\pi, \pi]$ has to be stored. This makes this metric a lightweight and efficient solution that will be later exploited for singularity avoidance.

5.2. *Action governor*

Consider a nominal control policy that computes the required torque, $\dot{\boldsymbol{h}}_c$, for a given attitude manoeuvre. Due to the redundancy of the system, the solution to

$$\dot{\boldsymbol{h}}_c = \boldsymbol{J}\dot{\boldsymbol{\gamma}}, \tag{30}$$

is the set

$$\mathcal{S} = \{\dot{\boldsymbol{\gamma}} \in \mathbb{R}^n : \dot{\boldsymbol{\gamma}} = \dot{\boldsymbol{\gamma}}_0 + \boldsymbol{N}\lambda\}, \tag{31}$$

where $\dot{\boldsymbol{\gamma}}_0 \in \mathbb{R}^n$ is the optimal energy solution, $\boldsymbol{N} \in \mathbb{R}^{n\times(m-\mathrm{rank}(\boldsymbol{J}))}$ is the normalized nullspace, and $\boldsymbol{\lambda} \in \mathbb{R}^{m-\mathrm{rank}(\boldsymbol{J})}$ is the scaling vector. Assuming that the gimbal rates are physically constrained to the interval

$$\mathcal{D} = \{\dot{\gamma}_i \in \mathbb{R} : |\dot{\gamma}_i| \leq \dot{\gamma}_{\max},\ \forall i = 1, ..., N\}, \tag{32}$$

where $\dot{\gamma}_{\max}$ denotes the maximum gimbal rate, the set of feasible solutions to (30) is given by

$$\mathcal{U} = \mathcal{S} \cap \mathcal{D}. \tag{33}$$

The optimal energy solution, $\dot{\boldsymbol{\gamma}}_0$, is obtained using the Moore-Penrose pseudoinverse, i.e.

$$\dot{\boldsymbol{\gamma}}_0 = \boldsymbol{J}^T(\boldsymbol{J}\boldsymbol{J}^T)^{-1}\dot{\boldsymbol{h}}_c. \tag{34}$$

Furthermore, to respect the physical limitations in (32), the optimal gimbal rates undergo a saturation function S, given by

$$S(\dot{\boldsymbol{\gamma}}_0) = \begin{cases} \dot{\boldsymbol{\gamma}}_0 & ,\text{if } \|\dot{\boldsymbol{\gamma}}_0\|_\infty < \dot{\gamma}_{\max}, \\ \dot{\gamma}_{\max}\dfrac{\dot{\boldsymbol{\gamma}}_0}{\|\dot{\boldsymbol{\gamma}}_0\|_\infty} & ,\text{if } \|\dot{\boldsymbol{\gamma}}_0\|_\infty \geq \dot{\gamma}_{\max}. \end{cases} \tag{35}$$

The optimal energy solution is usually sought as it allows to meet a control torque using the least control energy possible. However, there are situations where this solution may drive the system into a singularity. Therefore, an action governor is derived to monitor and modify, if necessary, the optimal gimbal rates in order to keep the system away from the singularities. Denoting the set of all $d \in \mathbb{R}_0^+$ by $\mathcal{X}$, a singularity influence region, $\mathcal{X}_0$, that the system ought to avoid, can be defined as

$$\mathcal{X}_0 = \{d \in \mathbb{R}_0^+ : d < \kappa\}, \tag{36}$$

where d represents the distance to the closest singularity, and $\kappa \in \mathbb{R}_0^+$ represents the distance threshold. Knowing this, the action governor can be formulated as an online constrained optimization problem of the form

$$\begin{aligned} \underset{\dot{\boldsymbol{\gamma}}(k)\,\in\,\mathcal{U}}{\text{minimize}} \quad & \|\dot{\boldsymbol{\gamma}}(k) - \dot{\boldsymbol{\gamma}}_0(k)\|_S^2 && \text{(37a)} \\ \text{subject to} \quad & \boldsymbol{\gamma}(k+1) = \boldsymbol{\gamma}(k) + T_s\dot{\boldsymbol{\gamma}}(k), && \text{(37b)} \\ & \boldsymbol{\gamma}(k+1) \in \mathcal{X}\backslash\mathcal{X}_0, && \text{(37c)} \end{aligned}$$

where $\mathcal{U}$ is the set of redundant solutions, T_s is the sampling time, $\boldsymbol{S} \succ 0$, and (37a) is employed to penalize the difference between the nominal gimbal rate command $\dot{\boldsymbol{\gamma}}_0(k)$ and the modified gimbal rates $\dot{\boldsymbol{\gamma}}(k)$ that satisfy (37c). For feasibility reasons, (37c) can be relaxed by being handled as a soft constraint in the cost function rather than a hard constraint. This can be done by using a penalty function $P_{\mathcal{X}_0}$, such that

$$P_{\mathcal{X}_0}(\boldsymbol{\gamma}) = \begin{cases} 0 & ,\text{if } \boldsymbol{\gamma} \in \mathcal{X}\backslash\mathcal{X}_0, \\ > 0 & ,\text{if } \boldsymbol{\gamma} \in \mathcal{X}_0. \end{cases} \tag{38}$$

Singularity avoidance is promoted by keeping the gimbal angles prediction, given by (37b), outside of the plane p (see Fig. 10). Consequently, the exclusion requirement is verified if

$$(\boldsymbol{\gamma}(k+1) - \boldsymbol{\gamma}_p(k))^T(\boldsymbol{\gamma}_s(k) - \boldsymbol{\gamma}_p(k)) \leq 0, \tag{39}$$

meaning that the boundary plane p, computed at the time instant k, is used for singularity avoidance at the time instant k+1. This allows for a reduction in the number of operations performed for singularity avoidance. In fact, the gimbal projection $\boldsymbol{\gamma}_p$ is obtained through a nonlinear expression. Therefore, to achieve linearity, this one cannot be updated inside the optimization problem. Using the penalty function $P_{\mathcal{X}_0}(\eta) = \max(\eta(k+1), 0)^2$, where

$$\eta(k+1) = (\boldsymbol{\gamma}(k+1) - \boldsymbol{\gamma}_p(k))^T(\boldsymbol{\gamma}_s(k) - \boldsymbol{\gamma}_p(k)), \tag{40}$$

it becomes possible to penalize any gimbal motion towards the inner side of the plane p.

5.3. *MPC-based allocation*

The previous approach relies on the numerical integration of the gimbal rates to obtain a one-step-ahead prediction of the gimbal angles. With this information, the system takes control actions that aim to avoid singularities while meeting the command torque. This method, however, is not effective in situations where it is impossible to avoid a singularity by computing the gimbal rates a single step ahead in time. Besides this, the solutions provided by this approach are commonly jerky, as the system is required to act immediately. Indeed, in some situations, the system has to be able to sense the proximity of the singularity far ahead in time in order to avoid it. This also allows for a reduction in the control energy used for dodging the singularity. Therefore, a new approach, that resorts to the model predictive control framework, is derived to overcome these limitations. This approach tackles the allocation problem by extending the prediction of the gimbal angles over a fixed prediction window. This provides the ability to anticipate

the proximity of a singularity region a few steps ahead in time, and consequently take control actions that lead to singularity-free configurations. To achieve this, a predictor is firstly derived to estimate the sequence of control torques, $\dot{\boldsymbol{H}}_c$, over the prediction window. The predictor uses the system model

$$\frac{d}{dt}\begin{pmatrix} q_0 \\ \boldsymbol{q} \\ \boldsymbol{\omega} \\ \boldsymbol{h} \end{pmatrix} = \begin{pmatrix} -\frac{1}{2}\boldsymbol{\omega}^T\boldsymbol{q} \\ \frac{1}{2}q_0\boldsymbol{I}_3\boldsymbol{\omega} - \frac{1}{2}\boldsymbol{S}(\boldsymbol{\omega})\boldsymbol{q} \\ \boldsymbol{I}_s^{-1}(-\dot{\boldsymbol{\omega}}\times\boldsymbol{I}_s\boldsymbol{\omega} - \dot{\boldsymbol{h}} - \boldsymbol{\omega}\times\boldsymbol{h} + \boldsymbol{\tau}) \\ \dot{\boldsymbol{h}}_c \end{pmatrix}. \tag{41}$$

It receives a sequence of attitude references $\boldsymbol{R}(k) = \big(\boldsymbol{r}(k), ..., \boldsymbol{r}(k+N_p)\big)$, where N_p denotes the prediction horizon, and combines (41) with the nominal controller to calculate the sequence of control torques, represented by $\dot{\boldsymbol{H}}_c(k) = \big(\dot{\boldsymbol{h}}_c(k), ..., \dot{\boldsymbol{h}}_c(k+N_p)\big)$, that are fed to the allocation MPC. This one aims to minimize the cost function

$$\begin{aligned}\mathcal{L} = \sum_{\tau=k}^{k+N_p} \Bigg(&\frac{1}{2}\|\dot{\boldsymbol{h}}(\tau) - \dot{\boldsymbol{h}}_c(\tau)\|_H^2 + \frac{1}{2}\|\dot{\boldsymbol{\gamma}}(\tau)\|_U^2 \\ &+ \frac{1}{2}\|\dot{\boldsymbol{\gamma}}(\tau) - \dot{\boldsymbol{\gamma}}(\tau-1)\|_M^2 + \frac{1}{2}\rho\max(\eta(\tau+1),0)^2\Bigg)\end{aligned} \tag{42}$$

subject to

$$\dot{\boldsymbol{h}}(\tau) = \boldsymbol{J}_\phi\dot{\boldsymbol{\gamma}}(\tau) + \boldsymbol{A}_\phi(\boldsymbol{\gamma}(\tau) - \boldsymbol{\gamma}_\phi(\tau)), \tag{43a}$$
$$\boldsymbol{\gamma}(\tau+1) = \boldsymbol{\gamma}(\tau) + T_s\dot{\boldsymbol{\gamma}}(\tau), \tag{43b}$$
$$|\dot{\boldsymbol{\gamma}}_i(\tau)| \leq \dot{\boldsymbol{\gamma}}_{\max}\ , \forall i = 1, ..., N, \tag{43c}$$
$$|\dot{\boldsymbol{\gamma}}_i(\tau) - \dot{\boldsymbol{\gamma}}_i(\tau-1)| \leq \Delta\dot{\boldsymbol{\gamma}}_{\max}\ , \forall i = 1, ..., N, \tag{43d}$$
$$\eta(\tau+1) = (\boldsymbol{\gamma}(\tau+1) - \boldsymbol{\gamma}_p(k))^T(\boldsymbol{\gamma}_s(k) - \boldsymbol{\gamma}_p(k)), \tag{43e}$$

where $\tau \in \{k, ..., k+N_p\}$. The optimization weights are the positive-definite matrices $\boldsymbol{H} \in \mathbb{R}^{m\times m}$, $\boldsymbol{U} \in \mathbb{R}^{n\times n}$, $\boldsymbol{M} \in \mathbb{R}^{n\times n}$, and the parameter $\rho \in \mathbb{R}^+$. The torque computation is linearized, in (43a), about the equilibrium $(\boldsymbol{\gamma}_\phi(\tau), \dot{\boldsymbol{\gamma}}_\phi(\tau))$ for all $\tau \in \{k, ..., k+N_p\}$, where the linearization matrices, $\boldsymbol{J}_\phi$ and $\boldsymbol{A}_\phi$, are given by

$$\boldsymbol{J}_\phi = \left.\frac{\partial\dot{\boldsymbol{h}}}{\partial\boldsymbol{\gamma}}\right|_{(\boldsymbol{\gamma}_\phi, \dot{\boldsymbol{\gamma}}_\phi)}, \qquad \boldsymbol{A}_\phi = \left.\frac{\partial\dot{\boldsymbol{h}}}{\partial\dot{\boldsymbol{\gamma}}}\right|_{(\boldsymbol{\gamma}_\phi, \dot{\boldsymbol{\gamma}}_\phi)}. \tag{44}$$

The equilibria used for torque linearization along the prediction horizon, at the time instant k, are defined by the sequence of gimbal states, $\boldsymbol{\Gamma}$, and the sequence of gimbal rates, $\dot{\boldsymbol{\Gamma}}$, computed at the time instant $k-1$. In addition, the equilibrium corresponding to the last prediction in the horizon, i.e. $(\boldsymbol{\gamma}_\phi(k+N_p), \dot{\boldsymbol{\gamma}}_\phi(k+N_p))$, is obtained by duplicating the last set of gimbal angles and gimbal rates in $\boldsymbol{\Gamma}(k-1)$ and $\dot{\boldsymbol{\Gamma}}(k-1)$, respectively. Note that the maximum gimbal rate variation, $\Delta\dot{\boldsymbol{\gamma}}_{\max}$, is obtained by multiplying the maximum gimbal acceleration, $\ddot{\boldsymbol{\gamma}}_{\max}$, with the sampling time, T_s. Similarly to Section 5.2, the exclusion plane p is computed for the time instant k, and kept constant along the horizon.

In short:

- The term $\frac{1}{2}\|\dot{\boldsymbol{h}}(\tau) - \dot{\boldsymbol{h}}_c(\tau)\|_H^2$ is used to penalize the mismatch between the control torque commands and the torques produced by the CMG system.
- The term $\frac{1}{2}\|\dot{\boldsymbol{\gamma}}(\tau)\|_U^2$ is used to minimize the control energy spent.
- The term $\frac{1}{2}\|\dot{\boldsymbol{\gamma}}(\tau) - \dot{\boldsymbol{\gamma}}(\tau-1)\|_M^2$ is another control energy metric. Yet, this term is used to penalize significant variations between consecutive gimbal inputs.
- Finally, the term $\frac{1}{2}\rho\max(\eta(\tau+1),0)^2$ is used for singularity avoidance.

Lastly, the optimization problem given by the cost function (42) and the set of constraints (43) is convex. This means that any solution is globally optimal and can be achieved at a very low computational expense. Indeed, (42) is given by the sum of four distinctive convex functions at every step in the horizon. The first three are quadratic whose Hessian matrices are positive-definite, and the last results from the composition of the affine map (43e) with the squared ReLU function ($f(x) = \max(x,0)^2$), that is known to be convex. Besides this, the equality constraints (43a) and (43b) are affine functions of $\dot{\boldsymbol{\gamma}}(\tau)$, and the inequality constraints (43c) and (43d) result from the composition of an affine map with the modulus function, that is also known to be convex.

6. Results

The MPC-based allocation strategy was tested in a small satellite model, with mass 180 kg, for different horizons and both with and without the presence of the singularity term in the cost function. The optimization weights were tuned to achieve optimal performance and the distance threshold parameter, κ, was set to 0.5 rad. In the following simulations, the prediction and the control horizons were set equal. The simulations were carried out for 90 s with a sampling time of 0.1 s. Lastly, an attitude reference consisting of constant references was defined as

$$(\phi, \theta, \psi) = \begin{cases} (0,0,0)\ \ [rad] & ,0 \leq t \leq 30, \\ (-25,20,0)\frac{\pi}{180}\ \ [rad] & ,30 < t \leq 60, \\ (0,0,0)\ \ [rad] & ,60 < t \leq 90. \end{cases} \tag{45}$$

The control torques and the actual torques produced by the system are provided in Figs. 11-13. For a horizon of one-time step, and without the use of the singularity term, it is obvious that the system meets a singularity at $t \approx 30$ s. This translates into a significant torque mismatch. For the same horizon, but using the singularity term, the torque mismatch is not as large as without the singularity term. Hence, the effectiveness of the singularity term is confirmed. For a horizon of five-time steps, i.e. 0.5 s, torque matching is verified.

The gimbal rates are shown in Figs. 14-16. For a horizon of one-time step, and without using the singularity term, the system requires a huge control effort to overcome the singularity effect. Even though the gimbal rates do not saturate, the gimbals accelerations do, which reflects in a large control energy. When the singularity term is added to the cost function, an overall reduction of the control energy is witnessed. Finally, the

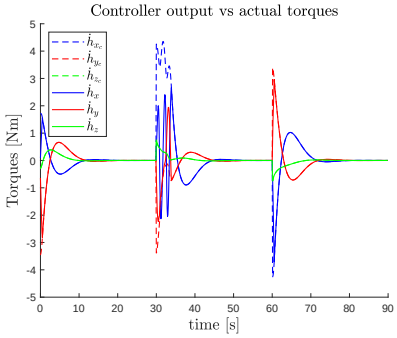

Fig. 11: Control torque vs. actual torque for a horizon of one-time step without the singularity term.

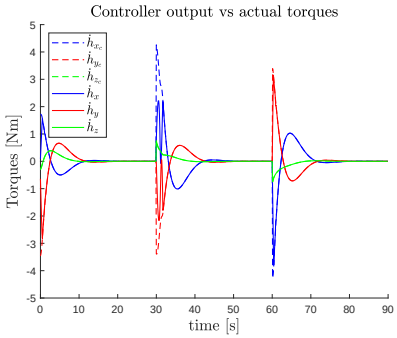

Fig. 12: Control torque vs. actual torque for a horizon of one-time step with the singularity term.

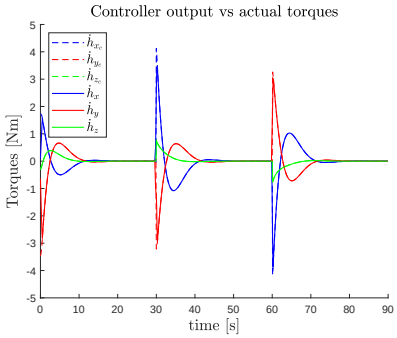

Fig. 13: Control torque vs. actual torque for a horizon of five-time steps with the singularity term.

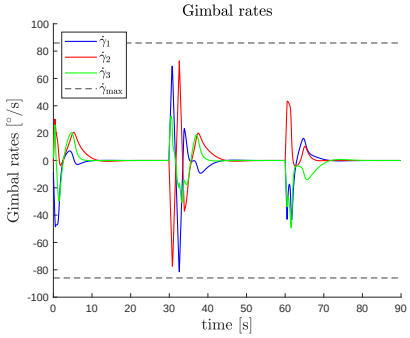

Fig. 14: Gimbal rates for a horizon of one-time step without the singularity term.

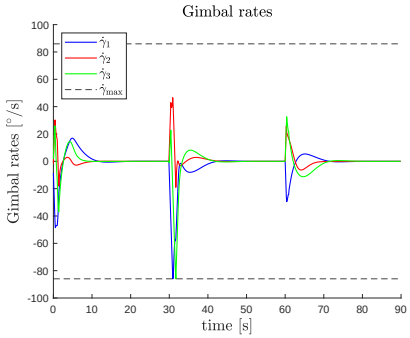

Fig. 15: Gimbal rates for a horizon of one-time step with the singularity term.

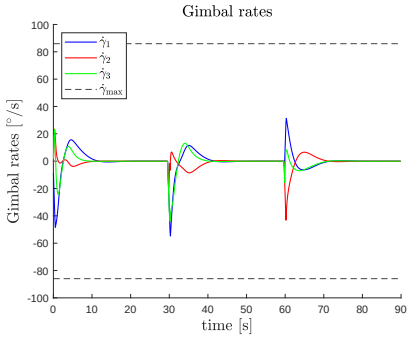

Fig. 16: Gimbal rates for a horizon of five-time steps with the singularity term.

gimbal rates are close to energy-minimal for a horizon of five-time steps.

The gimbal trajectory for the different horizons, without the use of the singularity term, is shown in Figs. 17 and 18. The plots validate the aforementioned conclusions. By increasing the MPC horizon, the system is able to predict the system's state a few steps ahead in time, and therefore anticipate the presence of a singularity. The closeness of a singularity is explicitly expressed in the cost function through the singularity term. However, the torque error term and the control energy terms also account for the existence of singularities implicitly. Since torque error is expected under the presence of a singularity, it is likely that by penalizing the torque error in the cost function, the system already performs some kind of singularity avoidance. The same reasoning applies to the control energy terms. Moreover, the hard constraints imposed on the gimbal rates and accelerations implicitly constrain the motion of the gimbals towards the singularities. Nevertheless, the system benefits from the singularity term, as seen before.

7. Conclusions

The long-standing singularity problem, that occurs in spacecrafts employing control moment gyros clusters, was addressed in this letter. The effect of a singularity in the system was carefully analyzed through the SVD of the Jacobian. It has been shown that for singular gimbal configurations, the Jacobian contains at least one null singular value that inhibits the creation of torque in the singular direction. This translates into a loss of controllability, that has an impact in the spacecraft's ACS.

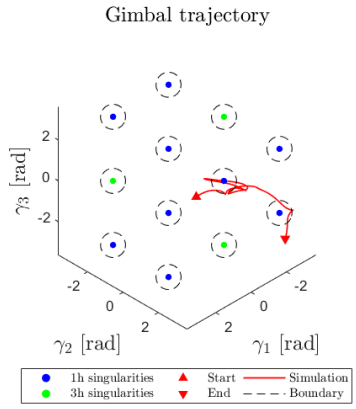

Fig. 17: Gimbal trajectory for a horizon of one-time step.

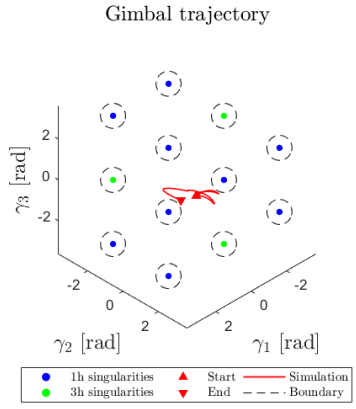

Fig. 18: Gimbal trajectory for a horizon of five-time steps.

To tackle this problem, an optimal allocation framework for singularity avoidance was proposed and validated in a simulation environment. Besides this, a new singularity metric was derived to perceive the proximity of a singularity. Contrary to common literature solutions, which are generally complex and computationally inefficient, this solution uses a rather simple function that estimates the Euclidean distance between the gimbals and the closest singularity. The advantage is that it can be integrated as a linear constraint in a convex optimization problem, resulting in a much lower computational cost.

Then, an MPC-based algorithm for CMG allocation was derived. With this approach, the system can predict the presence of a singularity a few steps ahead in time and take control actions that lead to singularity-free gimbal states. One could notice that the behaviour of the system improved as the prediction horizon increased. Besides this, the effectiveness of the novel singularity index was confirmed. Finally, the convergence to an optimal solution is guaranteed as convexity was achieved.

8. Future Work

The main guidelines for future work in this topic are as follows:

- The allocation algorithms should be validated in the presence of perturbations. These should include internal unmodelled perturbations, such as sensor noise and flexible vibration modes, and external perturbations, such as the gravity gradient, solar radiation pressure, and atmospheric drag.
- The proposed singularity index does not apply to every CMG system. In some cases, the singularity envelope cannot be described by lines, hence yielding to nonlinear representations that might be costly to store in an on-board computer. Therefore, convexification techniques to approximate the singularity envelope of a CMG array by a convex set should also be investigated.

References

[1] F. Leve, B. Hamilton, and M. Peck. *"Spacecraft Momentum Control Systems"*. Springer, 1^{st} edition, 2015. ISBN:978-3319225623.

[2] H. Leeghim, H. Bang, and J. Park. *"Singularity avoidance of control moment gyros by one-step ahead singularity index"*. *Acta Astronautica*, 64:935–945, May-June 2009. DOI: 10.1016/j.actaastro.2008.11.004.

[3] K. Takada and H. Kojima. *"Receding horizon control on steering of control moment gyro for fast attitude maneuvers"*. *Transactions of the Japan Society for Aeronautical and Space Sciences*, 52(175):1–10, May 2009. DOI: 10.2322/tjsass.52.1.

[4] H. Kojima, R. Nakamura, and S. Keshtkar. *"Model predictive steering control law for double gimbal scissored-pair control moment gyros"*. *Acta Astronautica*, 183(26), April 2021. DOI: 10.1016/j.actaastro.2021.03.023.

[5] Y. Ikeda, T. Nakajima, and Y. Chida. *"Attitude Control of Spacecraft by NMPC with Consideration of Singularity Avoidance of CMG"*. In *2012 IEEE 51st IEEE Conference on Decision and Control (CDC)*, Maui, HI, USA, December 2012. DOI: 10.1109/CDC.2012.6426827.

[6] A. Mony. *"RRT-Based Steering Law for Singularity Avoidance of Control Moment Gyros used for Spacecraft Target Acquisition"*. In *Indian Control Conference 2019*, IIT Hyderabad, December 2019. DOI: 10.1109/ICC47138.2019.9123199.

[7] C. Papakonstantinou, V. Lappas, H. Schaub, and V. Kostopoulos. *"Global Steering for Control Moment Gyroscope Clusters Using Heuristic Variable Search Techniques"*. *Journal of Spacecraft and Rockets*, 58(4):1–12, July-August 2021. DOI: 10.2514/1.A34850.

[8] C. Papakonstantinou, I. Daramouskas, V. Lappas, V. Moulianitis, and V. Kostopoulos. *"A Machine Learning Approach for Global Steering Control Moment Gyroscope Clusters"*. *Aerospace*, 9(3):164, March 2022. DOI: 10.3390/aerospace9030164.

[9] Y. Yang. *"Spacecraft Modeling, Attitude Determination and Control: Quaternion-based Approach"*. CRC Press, 1^{st} edition, 2019. ISBN:978-1138331501.

[10] R. Votel and D. Sinclair. *"Comparison of Control Moment Gyros and Reaction Wheels for Small Earth-Observing Satellites"*. In *26th Annual AIAA/USU Conference on Small Satellites*, Logan, UT, USA, August 2012.

[11] N. Li, K. Han, A. Girard, H. Tseng, D. Filev, and I. Kolmanovsky. *"Action Governor for Discrete-Time Linear Systems With Non-Convex Constraints"*. *IEEE Control Systems Letters*, 5(1):121–126, June 2020. DOI: 10.1109/LCSYS.2020.3000198.

[12] M. Schwenzer, M. Ay, T. Bergs, and D. Abel. *"Review on model predictive control: an engineering perspective"*. *The International Journal of Advanced Manufacturing Technology*, 117:1327–1349, August 2021. DOI: 10.1007/s00170-021-07682-3.

[13] O. Knill. *"Cauchy–Binet for pseudo-determinants"*. *Linear Algebra and its Applications*, 459:522–547, October 2014. DOI: 10.1016/j.laa.2014.07.013.